Slotted cylindrical shell for use as a compact wiggler

Robert L. Gluckstern
Physics Department, University of Maryland, College Park, Maryland 20742
(Received 22 April 1991)

A compact wiggler offers the opportunity to reach high free-electron-laser frequencies with an electron beam of modest energy. We analyze here the properties of a conducting cylinder, slotted periodically on alternate sides, for use as a compact wiggler. In particular, we obtain the current distribution on the cylindrical surface, from which we obtain the magnetic fields inside the cylinder. We then expand this field into its multipole components, as well as into its axial harmonics. The resulting orbit dynamics are explored, leading to preferred choices for some of the design parameters. Finally, we examine the major consequences of possible fabrication errors, which suggest the tolerances and/or necessary compensation mechanisms required for a satisfactory wiggler design.

I. INTRODUCTION

The early wigglers and undulators for use in a free-electron laser (FEL) were electromagnetic [1]. With the availability of high-remanant-field magnetic materials, most wiggler designs involved rare-earth-cobalt-type permanent magnets [2]. Current efforts to design high-field microwigglers have renewed interest in high-current, pulsed electromagnetic wigglers, since these should be capable of reaching higher fields than the permanent magnet wigglers.

The desire to operate FEL's at higher and higher frequencies creates an incentive to go to higher electron energies and/or shorter wiggler periods. Clearly a solution involving a compact or short-period wiggler avoids the cost of higher-energy accelerators. The challenge is to see if a design can be developed that generates strong enough field, is feasible to implement, and achieves the necessary tolerances.

One possible design involves using helical windings to produce the wiggler field [3]. Another possible wiggler, which is the subject of the present paper, consists of a cylindrical shell that is slotted periodically on alternate sides [4], as shown in Fig. 1. Among the attractions of this wiggler is that it produces plane-polarized FEL radiation, has high harmonic content in the wiggler field, which may be important in some applications, and consists, in principle, of tightly packed conductors, which should generate very high magnetic fields. In the present work, we derive the magnetic fields generated by passing a current through the slotted cylindrical shell. In particular, we assume that the shell is thin relative to its diameter and that the slots are thin relative to their spacing. We then solve the two-dimensional problem for the static current distribution in an "unrolled" unit cell. The magnetic fields within the cylinder that result from this current distribution on the cylindrical shell are then obtained. The electron-beam orbits in this magnetic field are then analyzed, including the effects of terms other than the main planar wiggler field. Finally, we explore methods to reduce or eliminate the undesired terms, and try to estimate the tolerances necessary to produce an appropriate wiggler field.

II. CONFORMAL TRANSFORMATION

If we unwrap the cylinder in Fig. 1, the two-dimensional current distribution will be approximately as shown in Fig. 2. The basic cell, which extends $\frac{1}{2}$ a period in the axial and azimuthal directions, is shown in Fig. 3. The segments (1)→(5) and (3)→(6) are perpendicular to the current flow and therefore can be thought of as equipotential lines, while the remaining boundary segments are parallel to the current flow. We therefore wish to solve the two-dimensional electrostatic problem where

$$\Phi(x,y)=\begin{cases} V \text{ on boundary line } (3)\rightarrow(6) & (2.1)\\ 0 \text{ on boundary line } (1)\rightarrow(5)\ . & (2.2)\end{cases}$$

In addition,

$$\frac{\partial\Phi}{\partial n}=0 \text{ on boundary lines } (5)\rightarrow(2)\rightarrow(3) \text{ and } (6)\rightarrow(4)\rightarrow(1)\ . \tag{2.3}$$

Let us consider the following conformal transformation:

$$\frac{dz}{dw}=-\frac{1}{\sqrt{(w+a)(w)(w-b)}}\ ,$$
$$z=\int_w^\infty \frac{1}{\sqrt{(w+a)(w)(w-b)}}dw\ . \tag{2.4}$$

The path in the w plane shown in Fig. 4 along the real axis from (1) ($w=\infty$) to (2) ($w=b$) to (3) ($w=0$) to (4) ($w=-a$) to (1) ($w=-\infty$), corresponds to the rectangle in the z plane in Fig. 3, with the lower-half w plane corresponding to the interior of the rectangle. Changing variable from w to b/s, the transformation can be written as

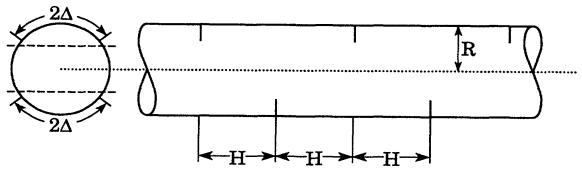

FIG. 1. Slotted cylindrical shell.

$$z=\int_0^{b/w}\frac{1}{\sqrt{s(1-s)(b+as)}}ds\ . \tag{2.5}$$

If we now let $s=\cos^2\theta$, we obtain

$$z=\frac{2}{\sqrt{a+b}}\int_{\sin^{-1}\sqrt{1-(b/w)}}^{\pi/2}\frac{1}{\sqrt{1-k^2\sin^2\theta}}d\theta\ ,$$
$$k^2=\frac{a}{a+b}\ . \tag{2.6}$$

Using the standard notation

$$F(\phi,k)=\int_0^{\phi}\frac{1}{\sqrt{1-k^2\sin^2\theta}}d\theta\ ,$$
$$K(k)=F\left[\frac{\pi}{2},k\right]\ , \tag{2.7}$$

we can write the transformation in terms of the incomplete elliptic integral, in the form

$$\sqrt{a+b}\,\frac{z}{2}=K(k)-F(\phi,k)\ ,$$
$$\phi=\sin^{-1}\sqrt{1-(b/w)}=\cos^{-1}\sqrt{b/w}\ . \tag{2.8}$$

The inverse of the elliptic integral is defined by

$$\chi=F(\phi,k),\quad \sin\phi=\mathrm{sn}(\chi)\ , \tag{2.9}$$

so that we can write the inverse transformation in terms of the elliptic function in the form

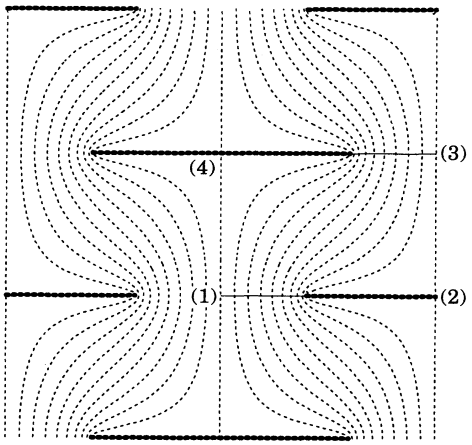

FIG. 2. Unrolled cylindrical shell with slots, showing current flow.

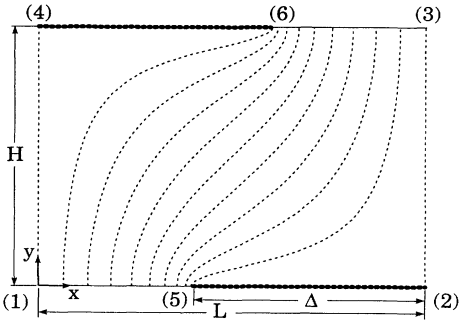

FIG. 3. Unit cell in the z plane.

$$\sqrt{1-(b/w)}=\mathrm{sn}\left[K(k)-\sqrt{a+b}\,\frac{z}{2}\right]\ . \tag{2.10}$$

The width and height of the rectangle can easily be shown to be given by

$$L=\pi R=z_2-z_1=\frac{2}{\sqrt{a+b}}K[\sqrt{a/(a+b)}] \tag{2.11}$$

and

$$H=|z_4-z_1|=\frac{2}{\sqrt{a+b}}K[\sqrt{b/(a+b)}]\ . \tag{2.12}$$

Let us now consider points (5) and (6) in the z plane such that the lines (6)→(4) and (5)→(2) are "metal plates" kept at potential V and 0, respectively. The parameter Δ is given by

$$\Delta=z_2-z_5=\int_b^q\frac{1}{\sqrt{(w+a)(w)(w-b)}}dw \tag{2.13}$$

and

$$\Delta=z_6-z_4=\int_{-a}^{-p}\frac{1}{\sqrt{(w+a)(-w)(b-w)}}dw\ . \tag{2.14}$$

Setting $w=b/s$ in Eq. (2.13), we find

$$\Delta=\int_{b/q}^{1}\frac{1}{\sqrt{s(1-s)(b+as)}}ds\ . \tag{2.15}$$

Setting $w=-as$ in Eq. (2.14), we find

$$\Delta=\int_{p/a}^{1}\frac{1}{\sqrt{s(1-s)(b+as)}}ds\ . \tag{2.16}$$

The equality of the two Δ's clearly requires

$$pq=ab \tag{2.17}$$

with

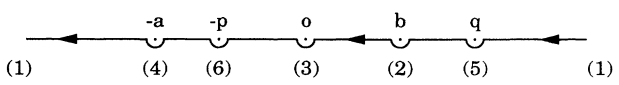

FIG. 4. Path in the w plane.

$$\Delta=\frac{2}{\sqrt{a+b}}F[\sin^{-1}\sqrt{1-(p/a)},k] \tag{2.18}$$

and

$$\sqrt{1-(p/a)}=\sqrt{1-(b/q)}=\mathrm{sn}\left[\sqrt{a+b}\,\frac{\Delta}{2}\right] . \tag{2.19}$$

The parameters a and b are determined from L and H by means of Eqs. (2.11) and (2.12) and the parameters p and q by means of Eq. (2.19) for specified Δ.

We next construct a second conformal transformation

$$\zeta=\int_w^\infty \frac{1}{\sqrt{(w+p)(w)(w-q)}}dw , \tag{2.20}$$

which converts the contour in the w plane into the rectangle in the ζ plane shown in Fig. 5, where the "metal plates" are the segments (1)→(5) and (6)→(3). The dimensions of the rectangle are

$$l=\xi_5-\xi_1=\frac{2}{\sqrt{p+q}}K[\sqrt{p/(p+q)}] , \tag{2.21}$$

$$h=\eta_6-\eta_1=\frac{2}{\sqrt{p+q}}K[\sqrt{q/(p+q)}] . \tag{2.22}$$

III. POTENTIAL DISTRIBUTION AND CURRENT DENSITY

The potential function corresponding to the boundary conditions in Fig. 5 is obviously

$$\Phi(\zeta)=\Phi(\xi,\eta)=\frac{V}{h}\eta=\frac{V}{h}\mathrm{Im}(\zeta) \tag{3.1}$$

and the lines of current flow are $\xi=$const. The transformation between ζ and w is obtained from Eq. (2.20) and is, in analogy with Eqs. (2.8) and (2.10),

$$\begin{aligned}&\frac{\sqrt{p+q}}{2}\zeta=K(\kappa)-F(\psi,\kappa) ,\\ &\psi=\sin^{-1}\sqrt{1-(q/w)} ,\\ &\kappa^2=\frac{p}{p+q} ,\end{aligned} \tag{3.2}$$

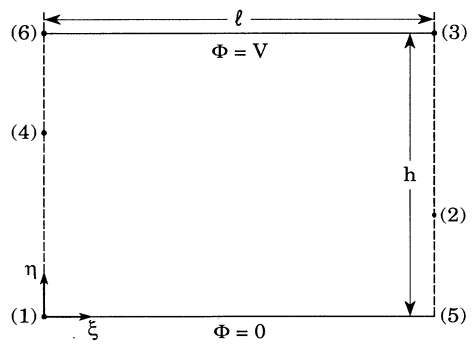

FIG. 5. Path in the ζ plane.

and

$$\sqrt{1-(q/w)}=\mathrm{sn}\left[K(\kappa)-\sqrt{p+q}\,\frac{\zeta}{2}\right] . \tag{3.3}$$

Use of Eqs. (2.8), (2.10), (3.2), and (3.3) allows us to relate $\zeta=\xi+i\eta$ to $z=x+iy$ (via $w=u+iv$), thereby providing the potential as a function of x and y and/or the lines of current flow. Explicit expressions for the field components are

$$\begin{aligned}E_x&=-\frac{\partial\Phi}{\partial y}=-\frac{V}{h}\frac{\partial n}{\partial x}\\ &=-\frac{\frac{\partial\eta}{\partial u}\frac{\partial y}{\partial v}-\frac{\partial y}{\partial u}\frac{\partial\eta}{\partial v}}{\frac{\partial x}{\partial u}\frac{\partial y}{\partial v}-\frac{\partial y}{\partial u}\frac{\partial x}{\partial v}} ,\end{aligned} \tag{3.4}$$

$$\begin{aligned}E_y&=-\frac{\partial\Phi}{\partial y}=-\frac{V}{h}\frac{\partial\eta}{\partial y}\\ &=-\frac{\frac{\partial x}{\partial u}\frac{\partial\eta}{\partial v}-\frac{\partial\eta}{\partial u}\frac{\partial x}{\partial v}}{\frac{\partial x}{\partial u}\frac{\partial y}{\partial v}-\frac{\partial y}{\partial u}\frac{\partial x}{\partial v}} .\end{aligned} \tag{3.5}$$

Using

$$\frac{dz}{dw}=-\frac{1}{\sqrt{(w+a)w(w-b)}}=\frac{\partial x}{\partial u}+i\frac{\partial y}{\partial u}=\frac{\partial y}{\partial v}-i\frac{\partial x}{\partial v} , \tag{3.6}$$

$$\frac{d\zeta}{dw}=-\frac{1}{\sqrt{(w+p)w(w-q)}}=\frac{\partial\xi}{\partial u}+i\frac{\partial\eta}{\partial u}=\frac{\partial\eta}{\partial v}-i\frac{\partial\xi}{\partial v} , \tag{3.7}$$

one can evaluate $\Phi(x,y)$, $E_x(x,y)$, and $E_y(x,y)$ with the help of w as a function of z given in Eq. (2.10).

We shall be particularly interested in the value of $\Phi(x,y)$ along the segment (5)→(2). It is obvious from Fig. 5 that

$$\Phi(x,0)=\frac{V}{h}\eta, \quad L-\Delta\le x\le L . \tag{3.8}$$

We can obtain η from Eq. (2.20) in the range $b\le w\le q$. The result for $\Phi(x,0)$ is

$$\begin{aligned}&\Phi(x,0)=\frac{V}{K(\kappa')}F[\sin^{-1}\sqrt{1-(w/q)},\kappa'] ,\\ &\kappa'^2=\frac{q}{p+q}=1-\kappa^2 .\end{aligned} \tag{3.9}$$

The relation between x and w is obtained from Eq. (2.6) and is

$$L-x=\frac{2}{\sqrt{a+b}}F[\sin^{-1}\sqrt{1-(b/w)},k] \tag{3.10}$$

or

$$\sqrt{1-(b/w)}=\mathrm{sn}\left[\frac{(L-x)\sqrt{a+b}}{2}\right] . \tag{3.11}$$

The current density is now obtained from $\mathbf{J}=\sigma\mathbf{E}$, so that the surface current density for a plate of thickness t and conductivity σ is

$$tJ_x=-\sigma t\frac{\partial\Phi}{\partial x},\quad tJ_y=-\sigma t\frac{\partial\Phi}{\partial y}\ . \tag{3.12}$$

The total current flowing in the y direction in the two cells which make up the cylindrical circumference is

$$I=2\int_0^L tJ_y dx=-2\sigma t\int_0^L dx\frac{\partial\Phi}{\partial y}\ . \tag{3.13}$$

But with the complex potential function

$$\Psi+i\Phi=\frac{V}{h}\zeta\ , \tag{3.14}$$

we have

$$\frac{\partial\Psi}{\partial y}=\frac{\partial\Phi}{\partial x},\quad \frac{\partial\Psi}{\partial x}=-\frac{\partial\Phi}{\partial y} \tag{3.15}$$

and

$$I=2\sigma t\int_0^L dx\frac{\partial\Psi}{\partial x}=2\sigma t[\Psi(L)-\Psi(0)]=2\sigma t\frac{Vl}{h}\ . \tag{3.16}$$

Thus, the resistance per axial length H is

$$R_H=\frac{h}{2lt\sigma} \tag{3.17}$$

and the power dissipation per axial length H is

$$P=\frac{V^2}{R_H}=\frac{2V^2lt\sigma}{h}\ . \tag{3.18}$$

The power dissipation distribution, of interest in determining the transient and steady-state temperature behavior, is readily obtained from the conformal map, since

$$|E|^2=(\nabla\Phi)^2=\frac{V^2}{h^2}\left|\frac{d\zeta}{dz}\right|^2=\frac{V^2}{h^2}\frac{|d\zeta/dw|^2}{|dz/dw|^2}\ , \tag{3.19}$$

leading to

$$\frac{dP}{dA}=\sigma t|E|^2=\frac{(w+a)(w-b)}{(w+p)(w-q)}\frac{V^2\sigma t}{h^2}$$
$$=\frac{P}{2hl}\frac{(w+a)(w-b)}{(w+p)(w-q)}\ . \tag{3.20}$$

The power density in the (x,y) plane near the spot corresponding to the singularity at $z=z_6$ $(w=-p)$ is

$$\frac{dP}{dA}=\frac{P}{2hl}\frac{(a-p)(b+p)}{(p+q)}\frac{1}{w+p}\ . \tag{3.21}$$

But the transformation from the z plane to the w plane near $w=-p$ is, according to Eq. (2.4),

$$z-z_6\cong\frac{w+p}{\sqrt{p(b+p)(a-p)}}\ , \tag{3.22}$$

so that

$$\left|\frac{dP}{dA}\right|_6\cong\frac{P}{2hl}\frac{\sqrt{(a-p)(b+p)}}{(p+q)\sqrt{p}}$$
$$\times\frac{1}{\sqrt{(x-x_6)^2+(y-y_6)^2}}\ . \tag{3.23}$$

IV. FOURIER EXPANSION OF CURRENT DENSITY

We now have the ability to calculate the potential $\Phi(x,y)$ in the cell shown in Fig. 2. Specifically, Eq. (3.1) gives Φ as a function of ζ, Eqs. (3.2) and (3.3) connect ζ and w, and Eqs. (2.8) and (2.10) connect w and z. We now wish to expand $\Phi(x,y)$ into a double Fourier series in x and y, taking into account the symmetries and periodicities displayed in Fig. 2.

Our first step is to subtract the term linear in y from the potential. Specifically, we form the function $\chi(x,y)$ defined by

$$\chi(x,y)=\Phi(x,y)-\frac{Vy}{H}\ , \tag{4.1}$$

which is now periodic in x (period $2L$) and y (period $2H$) with the following symmetries evident in Figs. 1 and 2:

$$\chi(-x,y)=\chi(x,y)\ , \tag{4.2}$$

$$\chi(x,-y)=-\chi(x,y)\ , \tag{4.3}$$

$$\chi(L-x,H-y)=-\chi(x,y)\ . \tag{4.4}$$

If we also require $\nabla^2\chi(x,y)=0$, $\chi(x,y)$ can be expanded in the region $-L\le x\le L$, $0<y<H$, as

$$\chi(x,y)=\sum_{\substack{n=0\\ \text{even}}}^{\infty}C_n\cos\left[\frac{n\pi x}{L}\right]\sinh\left[\frac{n\pi}{L}\left[\frac{H}{2}-y\right]\right]$$
$$+\sum_{\substack{n=1\\ \text{odd}}}^{\infty}D_n\cos\left[\frac{n\pi x}{L}\right]\cosh\left[\frac{n\pi}{L}\left[\frac{H}{2}-y\right]\right]\ . \tag{4.5}$$

The separation into $n=$even,odd is required to satisfy Eqs. (4.2) and (4.4).

The coefficients C_n and D_n can readily be obtained from $\chi(x,0)=\Phi(x,0+)$, where $y=0+$ designates the potential on the positive y side of the surface $y=0$. This designation is needed because $\Psi(x,y)$ and $\chi(x,y)$ are discontinuous on the segments (5)→(2), (4)→(6), etc. Specifically, we find

$$C_n\sinh\left[\frac{n\pi H}{2L}\right]=2Q_nV,\quad n\text{ even} \tag{4.6}$$

$$D_n\cosh\left[\frac{n\pi H}{2L}\right]=2Q_nV,\quad n\text{ odd}\ , \tag{4.7}$$

where

$$(1+\delta_{n0})Q_n=\frac{1}{LV}\int_{L-\Delta}^{L}dx\ \Phi(x,0+)\cos\left[\frac{n\pi x}{L}\right]$$
$$=\frac{(-1)^n}{LV}\int_0^{\Delta}dx\ \Phi(L-x,0+)\cos\left[\frac{n\pi x}{L}\right] \tag{4.8}$$

are the Fourier coefficients of the expansion of $\Phi(x,0+)$ in the region $-L\le x\le L$. We then have

$$\chi(x,y)=2V\sum_{\substack{n=2\\ \text{even}}}^{\infty} Q_n\cos\left[\frac{n\pi x}{L}\right]\frac{\sinh[(n\pi/2L)(H-2y)]}{\sinh(n\pi H/2L)}$$

$$+2V\sum_{\substack{n=1\\ \text{odd}}}^{\infty} Q_n\left[\cos\frac{n\pi x}{L}\right]\frac{\cosh[(n\pi/2L)/(H-2y)]}{\cosh(n\pi H/2L)}+2VQ_0\left[1-\frac{2y}{H}\right], \tag{4.9}$$

where the last term comes from the $n=0$ term in the sum. If we now use Eq. (4.1) to obtain $\Phi(x,y)$ and write

$$J_x=-\sigma\frac{\partial\Phi}{\partial x},\quad J_y=-\sigma\frac{\partial\Phi}{\partial y}, \tag{4.10}$$

we find

$$\frac{J_x}{\sigma V}=2\sum_{\substack{n=2\\ \text{even}}}^{\infty}\frac{n\pi Q_n}{L}\sin\left[\frac{n\pi x}{L}\right]\frac{\sinh[(n\pi/2L)(H-2y)]}{\sinh(n\pi H/2L)}$$

$$+2\sum_{\substack{n=1\\ \text{odd}}}^{\infty}\frac{n\pi Q_n}{L}\sin\left[\frac{n\pi x}{L}\right]\times\frac{\cosh[(n\pi/2L)(H-2y)]}{\cosh(n\pi H/2L)} \tag{4.11}$$

and

$$\frac{J_y}{\sigma V}=\frac{1}{H}+\frac{4Q_0}{H}+2\sum_{\substack{n=2\\ \text{even}}}^{\infty}\frac{n\pi Q_n}{L}\cos\left[\frac{n\pi x}{L}\right]\times\frac{\cosh[(n\pi/2L)(H-2y)]}{\sinh(n\pi H/2L)}$$

$$+2\sum_{\substack{n=1\\ \text{odd}}}^{\infty}\frac{n\pi Q_n}{L}\cos\left[\frac{n\pi x}{L}\right]\times\frac{\sinh[(n\pi/2L)(H-2y)]}{\cosh(n\pi H/2L)}. \tag{4.12}$$

We now expand $\sinh[(n\pi/2L)(H-2y)]$ and $\cosh[(n\pi/2L)(H-2y)]$ into a Fourier series in y (period $2H$), taking into account the approximate symmetry for J_x and J_y corresponding to Eq. (4.3). The result is

$$\frac{J_x}{\sigma V}=\frac{8}{H}\sum_{\substack{m\geq 1\\ m+n\\ \text{even}}}\sum_{n\geq 1} Q_n\sin\left[\frac{n\pi x}{L}\right]\sin\left[\frac{m\pi y}{H}\right]\times\frac{m(nH/L)}{m^2+(nH/L)^2} \tag{4.13}$$

and

$$\frac{J_y}{\sigma V}=-\left[\frac{1-4Q_0}{H}\right]+\frac{4}{H}\sum_{\substack{n=2\\ \text{even}}}^{\infty} Q_n\cos\left[\frac{n\pi x}{L}\right]+\frac{8}{H}\sum_{\substack{m\geq 1\\ m+n\\ \text{even}}}\sum_{n\geq 1} Q_n\cos\left[\frac{n\pi x}{L}\right]\cos\left[\frac{m\pi y}{H}\right]\times\frac{(nH/L)^2}{m^2+(nH/L)^2}. \tag{4.14}$$

By expanding into a Fourier series *after* taking the gradient of $\chi(x,y)$ to obtain the components of the current, we have avoided the singularity caused by the discontinuity in $\Phi(x,y)$ at $y=0,\pm H,\pm 2H$, etc., which would have occurred by first expanding $\chi(x,y)$ into a double Fourier series and then taking the gradient.

V. MAGNETIC FIELD WITHIN THE CYLINDRICAL SHELL

We now roll the shell back up, assuming that the current distribution remains as given by Eqs. (4.13) and (4.14) in the cylindrical coordinate system, where

$$x\to R\theta,\quad y\to z,\quad L=\pi R,\quad H=\pi/k,\quad L/H\equiv\rho=kR. \tag{5.1}$$

We can therefore write

$$J_\theta=\frac{8\sigma kV}{\pi}\sum_{\substack{m\geq 1\\ m+n\\ \text{even}}}^{\infty}\sum_{n\geq 1}^{\infty}\frac{mn\rho Q_n}{n^2+m^2\rho^2}\sin(n\theta)\sin(mkz), \tag{5.2}$$

$$J_z=-\frac{\sigma kV}{\pi}(1-4Q_0)+\frac{4\sigma kV}{\pi}\sum_{n=2}^{\infty}Q_n\cos(n\theta)+\frac{8\sigma kV}{\pi}\sum_{\substack{m\geq 1\\ m+n\\ \text{even}}}^{\infty}\sum_{n\geq 1}^{\infty}\frac{n^2Q_n}{n^2+m^2\rho^2}\cos(n\theta)\cos(mkz). \tag{5.3}$$

We shall proceed by obtaining the scalar magnetic potential inside and outside the cylinder. Since $\sin(n\theta)$, $\cos(n\theta)$, and $\sin(mkz)$, $\cos(mkz)$ represent complete sets in θ and z, the individual coefficients for each m and n must match. Moreover, since $\nabla^2\Psi_{\text{mag}}=0$, the radial dependence of each term must be the Bessel functions $I_n(mkr)$ inside the cylinder and $K_n(mkr)$ out-

side the cylinder, with the requirement that $H_r=\partial\Psi_{\rm mag}/\partial r$ be continuous at $r=R$. We therefore write

$$\Psi_{\rm mag}=V\sum_{\substack{n=2\\ \text{even}}}^{\infty}\frac{\lambda_{0n}\sin(n\theta)}{4\rho}\times\begin{cases}-r^nR^{-n}, & r<R\\ r^{-n}R^n, & r>R\end{cases}+V\sum_{\substack{m\geq 1\\ m+n\\ \text{even}}}^{\infty}\sum_{n\geq 1}^{\infty}m\lambda_{mn}\sin(n\theta)\cos(mkz)\times\begin{cases}I_n(mkr)K_n'(m\rho), & r<R\\ K_n(mkr)I_n'(m\rho), & r>R\end{cases}\tag{5.4}$$

where $\mathbf{B}=\mu\nabla\Psi_{\rm mag}$, and where we have written the $m=0$ term separately. The discontinuity in H_θ at $r=R$ is tJ_z and the discontinuity in H_z at $r=R$ is $-tJ_\theta$. The two condition are consistent with one another, since $\mathbf{J}$ in Eqs. (5.2) and (5.3) explicitly satisfies $\nabla\cdot\mathbf{J}=0$. We therefore obtain

$$\lambda_{mn}=\frac{8\sigma t}{\pi}\rho^2\frac{nQ_n}{n^2+m^2\rho^2}\ ,\qquad m\geq 0,\ n\geq 1,\ m+n\ \text{even}\ .\tag{5.5}$$

We have omitted the uniform current term in Eq. (5.3) since it produces no field inside the cylindrical shell. However, it must be included in any calculation of forces on the cylinder.

The field components inside the cylindrical shell are obtained by taking the gradient of Eq. (5.4). We will do this in rectangular coordinates only for the leading terms in powers of r. Specifically, we write

$$\Psi_{\rm mag}(x,y,z)=-\frac{\lambda_{02}V2xy}{4\rho R^2}+V\sum_{\substack{m=1\\ \text{odd}}}^{\infty}m\lambda_{m1}\cos(mkz)K_1'(m\rho)\frac{mky}{2}\left[1+\frac{m^2k^2(x^2+y^2)}{8}\right]+V\sum_{\substack{m=1\\ \text{odd}}}^{\infty}m\lambda_{m3}\cos(mkz)K_3'(m\rho)\frac{m^3k^3}{48}(3x^2y-y^3)+V\sum_{\substack{m=2\\ \text{even}}}^{\infty}m\lambda_{m2}\cos(mkz)K_2'(m\rho)\frac{m^2k^2}{8}2xy\tag{5.6}$$

from which we obtain the dipole wiggler term

$$\Psi_{\rm mag}^{\rm dipole}=\Psi_0\frac{y}{R}\sum_{\substack{m=1\\ \text{odd}}}^{\infty}\alpha_m^d\cos(mkz)\ ,\tag{5.7}$$

the quadrupole term

$$\Psi_{\rm mag}^{\rm quad}=\Psi_0\frac{xy}{R^2}\frac{Q_2}{Q_1}\sum_{\substack{m=0\\ \text{even}}}^{\infty}\alpha_m^q\cos(mkz)\ ,\tag{5.8}$$

and the sextupole terms

$$\Psi_{\rm mag}^{\rm sext}=\Psi_0\left[\frac{y(3x^2-y^2)}{R^3}\frac{Q_3}{Q_1}\sum_{\substack{m=1\\ \text{odd}}}^{\infty}\alpha_m^s\cos(mkz)+\frac{y(x^2+y^2)\rho^2}{8R^3}\sum_{\substack{m=1\\ \text{odd}}}^{\infty}m^2\alpha_m^d\cos(mkz)\right].\tag{5.9}$$

Here

$$\Psi_0=\frac{\rho}{2}\lambda_{11}VK_1'(\rho)=\frac{4V\sigma t\rho^3K_1'(\rho)}{\pi(1+\rho^2)}Q_1\ ,\tag{5.10}$$

$$\alpha_m^d=\frac{m^2\lambda_{m1}K_1'(m\rho)}{\lambda_{11}K_1'(\rho)}=\frac{m^2(1+\rho^2)K_1'(m\rho)}{(1+m^2\rho^2)K_1'(\rho)},\quad m\geq 1\ \text{odd}\tag{5.11}$$

$$\alpha_0^q=-\frac{\lambda_{02}}{\rho^2\lambda_{11}K_1'(\rho)}=-\frac{1+\rho^2}{\rho^2K_1'(\rho)}\ ,\tag{5.12}$$

$$\alpha_m^q=\frac{m^3\rho}{2}\frac{\lambda_{m2}K_2'(m\rho)}{\lambda_{11}K_1'(\rho)}\frac{Q_1}{Q_2}=\frac{m^3\rho(1+\rho^2)K_2'(m\rho)}{(4+m^2\rho^2)K_1'(\rho)},\quad m\geq 2\ \text{even}\tag{5.13}$$

$$\alpha_m^s=\frac{m^4\rho^2}{24}\frac{\lambda_{m3}K_3'(m\rho)}{\lambda_{11}K_1'(\rho)}\frac{Q_1}{Q_3}=\frac{m^4\rho^2(1+\rho^2)K_3'(m\rho)}{8(9+m^2\rho^2)K_1'(\rho)},\quad m\geq 1\ \text{odd}\ .\tag{5.14}$$

The components of $\mathbf{B}$ are obtained by taking the gradient of Eqs. (5.7)–(5.9). Note that our normalization has been chosen so that $\alpha_1^q=1$, and that for $\rho\sim 1$, all coefficients α_m are of order 1.

The first harmonic ($m=1$) wiggler parameter

$$K=\frac{eB_y^{\max}}{m_0ck_w}=\frac{\mu e\Psi_0}{m_0ck_wR}\tag{5.15}$$

is given by

$$K=\frac{\mu eV}{2mc}\lambda_{11}=\frac{4\mu\sigma t}{\pi}\frac{Ve}{m_0c}\frac{Q_1\rho^2K_1'(\rho)}{1+\rho^2}\ ,\tag{5.16}$$

where m_0 is the electron mass. Using Eq (3.16), we can express K in terms of the current and dimensionless parameters as

$$K=\frac{Q_1\rho^2K_1'(\rho)}{1+\rho^2}\frac{h}{l}\frac{I}{I_0}\ , \tag{5.17}$$

where $I_0=\pi m_0c^2/2eZ_0=2.13$ kA, with $Z_0=377\ \Omega$. Here

$$\rho=L/H=k_wR\ , \tag{5.18}$$

where the subscript w has been added to the wiggler wave number to conform to the usual notation, with $k_w=2\pi/\lambda_w=\pi/H$. Since our analysis will not involve the frequency of the radiation, we will once again drop the subscript w in the next section.

As a final point, we can calculate the total current by integrating Eq. (5.3) over θ, obtaining

$$I=2\pi Rt\frac{\sigma kV}{\pi}(1-4Q_0)=2\rho\sigma Vt(1-4Q_0)\ . \tag{5.19}$$

Comparison with Eq. (3.16) allows us to write

$$\frac{l}{h}=\rho(1-4Q_0)=\frac{L}{H}(1-4Q_0)\ . \tag{5.20}$$

This relation is used to check the accuracy of our numerical calculations.

VI. ORBIT DYNAMICS

The electron motion in the magnetic field corresponding to Eqs. (5.7), (5.8), and (5.9) is obtained from the equations of motion

$$\ddot{x}=\frac{e}{m_0\gamma}(\dot{y}B_z-\dot{z}B_y),\quad \ddot{y}=\frac{e}{m_0\gamma}(\dot{z}B_x-\dot{x}B_z)\ . \tag{6.1}$$

If we change independent variable to z, we can write

$$\frac{d}{dz}\dot{x}=\frac{e}{m_0\gamma}(y'B_z-B_y),\quad \frac{d}{dz}\dot{y}=\frac{e}{m_0\gamma}(B_x-x'B_z)\ , \tag{6.2}$$

where the prime indicates differentiation with respect to z. Using $\dot{x}=x'\dot{z}$, $\dot{y}=y'\dot{z}$, and $\dot{z}\cong c(1-x'^2/2-y'^2/2)$, valid for $\gamma\gg1$, it is not difficult to see that the difference between $\dot{z}/c$ and 1 is of order γ^{-2} for a wiggler parameter K of order 1. We shall therefore set $\dot{z}=c$ to obtain

$$x''\cong\frac{e}{m_0\gamma c}(y'B_z-B_y)\ , \tag{6.3}$$

$$y''\cong\frac{e}{m_0\gamma c}(B_x-x'B_z)\ . \tag{6.4}$$

The first harmonic wiggler field in Eq. (5.7) has a magnitude Ψ_0/R since α_m^d has been normalized so that $\alpha_1^d=1$. The wiggler parameter K is therefore

$$K=\frac{\mu e}{m_0ck}\frac{\Psi_0}{R}=\frac{\mu e\Psi_0}{m_0c\rho}\ . \tag{6.5}$$

The coefficient on the right-hand side of Eqs. (6.3) and (6.4) is therefore proportional to

$$\frac{\mu e}{m_0\gamma c}\frac{\Psi_0}{R}=\frac{K\rho}{\gamma R}\equiv\frac{1}{A}\ , \tag{6.6}$$

where A is the radius of curvature of the electrons in the first harmonic maximum wiggler field.

The procedure we shall follow is to solve (6.3) in lowest order in x for $y=0$ to obtain the main wiggler motion. Equation (6.4) will then be linearized in y and solved for the oscillatory motion, averaging over the main wiggler motion in x. Finally, we will use Eq. (6.3) with $y=0$, and we will include higher-order terms in x/R to determine the presence of any focusing or defocusing forces in the x direction.

We therefore start with Eq. (6.3) for $y=0$, writing

$$x''=-\frac{1}{A}\left[\sum_{\substack{m=1\\ \text{odd}}}^{\infty}\alpha_m^d\cos(mkz)+\frac{x}{R}\frac{Q_2}{Q_1}\sum_{\substack{m=0\\ \text{even}}}^{\infty}\alpha_m^q\cos(mkz)+\frac{x^2}{R^2}\sum_{\substack{m=1\\ \text{odd}}}^{\infty}\left[3\alpha_m^s\frac{Q_3}{Q_1}+m^2\alpha_m^d\right]\cos(mkz)\right]\ . \tag{6.7}$$

Keeping only the first term on the right-hand side, we find

$$\frac{x}{R}\cong\frac{1}{k^2AR}\sum_{\substack{m=1\\ \text{odd}}}^{\infty}\frac{\alpha_m^d\cos(mkz)}{m^2}=\frac{R}{\rho^2A}\sum_{\substack{m=1\\ \text{odd}}}^{\infty}\frac{\alpha_m^d\cos(mkz)}{m^2}\ , \tag{6.8}$$

where $\rho=kR$ and K are of order 1, and where x/R and R/A are of order $1/\gamma$.

The linearized equation for the y motion is

$$y''=-G_yy\ , \tag{6.9}$$

where

$$G_y=-\frac{1}{AR}\left[\frac{Q_2}{Q_1}\sum_{\substack{m=0\\ \text{even}}}^{\infty}\alpha_m^q\cos(mkz)+\frac{2x}{R}\sum_{\substack{m=1\\ \text{odd}}}^{\infty}\left[3\alpha_m^s\frac{Q_3}{Q_1}+m^2\alpha_m^d\right]\cos(mkz)\right.$$
$$+\rho x'\sum_{\substack{m=1\\ \text{odd}}}^{\infty}m\alpha_m^d\sin(mkz)+\frac{\rho xx'}{R}\frac{Q_2}{Q_1}\sum_{\substack{m=2\\ \text{even}}}^{\infty}m\alpha_m^q\sin(mkz)$$
$$\left.+\frac{\rho x^2x'}{R^2}\sum_{\substack{m=1\\ \text{odd}}}^{\infty}m\left[3\alpha_m^s\frac{Q_3}{Q_1}+m^2\alpha_m^d\right]\sin(mkz)\right]\ . \tag{6.10}$$

In calculating the value of G_y averaged over the wiggler motion in the x direction, we can integrate by parts, obtaining in lowest orders in γ^{-1}

$$\langle G_y \rangle = -\frac{\alpha_0^q}{AR}\frac{Q_2}{Q_1} + \frac{\rho^2}{AR}\sum_{\substack{m=1\\ \text{odd}}}^{\infty} m^2\alpha_m^d \left\langle \frac{x}{R}\cos(mkz)\right\rangle - \frac{2}{AR}\sum_{\substack{m=1\\ \text{odd}}}^{\infty}\left[3\alpha_m^s\frac{Q_3}{Q_1} + m^2\alpha_m^d\right] \times \left\langle \frac{x}{R}\cos(mkz)\right\rangle . \tag{6.11}$$

Using Eq. (6.8) we find

$$\langle G_y \rangle = \frac{\alpha^d}{2A^2} - \frac{\alpha_0^q}{AR}\frac{Q_2}{Q_1} - \frac{\alpha^s}{A^2}\frac{Q_3}{Q_1} - \frac{\alpha^d}{8A^2} , \tag{6.12}$$

where

$$\alpha^d = \sum_{\substack{m=1\\ \text{odd}}}^{\infty}(\alpha_m^d)^2, \quad \alpha^s = \frac{3}{\rho^2}\sum_{\substack{m=1\\ \text{odd}}}^{\infty}\frac{\alpha_m^d\alpha_m^s}{m^2} . \tag{6.13}$$

The focusing in the x direction can be obtained by writing

$$\frac{x}{R} = \frac{R}{\rho^2 A}\sum_{\substack{m=1\\ \text{odd}}}^{\infty}\frac{\alpha_m^d\cos(mkz)}{m^2} + u \tag{6.14}$$

and linearizing in u. In this way we obtain

$$u'' = -G_x u , \tag{6.15}$$

where

$$G_x = \frac{1}{AR}\left[\sum_{\substack{m=0\\ \text{even}}}^{\infty}\alpha_m^q\frac{Q_2}{Q_1}\cos(mkz) + \frac{2x}{R}\sum_{\substack{m=1\\ \text{odd}}}^{\infty}\left[3\alpha_m^s\frac{Q_3}{Q_1} + m^2\alpha_m^d\right]\cos(mkz)\right] . \tag{6.16}$$

Averaging over the wiggler motion in the x direction, we obtain

$$\langle G_x \rangle = \frac{\alpha_0^q}{AR}\frac{Q_2}{Q_1} + \frac{\alpha^s}{A^2}\frac{Q_3}{Q_1} + \frac{\alpha^d}{8A^2} . \tag{6.17}$$

Clearly, from Eqs. (6.12) and (6.16), we find

$$\langle G_x \rangle + \langle G_y \rangle = \frac{\alpha^d}{2A^2} . \tag{6.18}$$

The cancellation of the quadrupole and sextupole coefficients in Eq. (6.18) is related to a consequence of Earnshaw's theorem [5]. Specifically, the sum of the force gradients in the x and y directions must be the negative of the force gradient in the z direction, which comes from the average of the z gradient of $x'B_y e/m_0\gamma c$. Using B_y from Eq. (5.7) and obtaining x' from Eq. (6.8), one obtains $\alpha^d/2A^2$ for the negative of $\langle G_z \rangle$, in agreement with Eq. (6.18).

Additional terms in the multipole expansions in Eqs. (6.10) and (6.16) can be obtained. It is easy to show that these lead to octupole terms in Eqs. (6.12) and (6.17) which are proportional to R/A^3 and decapole terms proportional to R^2/A^4. Thus, each higher-order multipole introduces a term with one higher power of R/A compared with the sextupole term. Since $R/A \sim \gamma^{-1} \ll 1$, these terms are neglected.

It is clear from Eqs. (6.12) and (6.16) that the largest term for $A \gg R$ is the quadrupole term. For this reason, a design in which both the x and y motions are stable can be achieved if Q_2 can be made to vanish. We will show later that $[\Phi(x,0+)]^2$ is very nearly linear in $(L-x)^2$. As a result, Q_2, defined in Eq. (4.8) is very nearly proportional to $J_1(2\pi\Delta/L)$. By choosing $\Delta/L = 3.83/2\pi \cong 0.61$, we can greatly reduce the impact of the quadrupole term in Eqs. (6.12) and (6.16). In fact, we may be able to choose Δ/L in a way which, taking the sextupole terms into account, allows us to balance the focusing forces so that

$$\langle G_x \rangle \cong \langle G_y \rangle \cong \frac{\alpha^d}{4A^2} , \tag{6.19}$$

where α^d is given in Eq. (6.13).

At this point we note that we have ignored terms which couple the oscillations in the x and y directions. Their effect is to exchange energy between the two oscillations over a distance which is *large* compared to A, and which is therefore not important for wigglers whose length is comparable with A.

VII. NUMERICAL VALUES

The choice of parameters depends on many factors, most of which are beyond the scope of the present work. We start by selecting a particular radiation wavelength and an upper limit to the electron energy. Since

$$\lambda = \frac{\lambda_w(1+K^2/2)}{2\gamma^2} \tag{7.1}$$

and we wish to keep K of order 1, Eq. (7.1) prescribes λ_w, which is of order a few mm in the present plans.

The next parameter to be chosen is R. Clearly, the smaller R is the larger will be the wiggler field. But the inner radius of the cylinder must be large enough to contain the beam. The maximum field for a given wiggler current and fixed k_w is given in Eq. (5.18). Specifically, we find

$$\frac{eB_y^{\max}}{m_0 c} = k_w K = k_w f_{\max}\frac{I}{I_0} , \tag{7.2}$$

where

$$f_{\max} = \frac{Q_1 h}{l}\frac{\rho^2 K_1'(\rho)}{1+\rho^2} = \frac{Q_1}{\rho(1-4Q_0)}\frac{\rho^2 K_1'(\rho)}{1+\rho^2} = \frac{K}{I}I_0 . \tag{7.3}$$

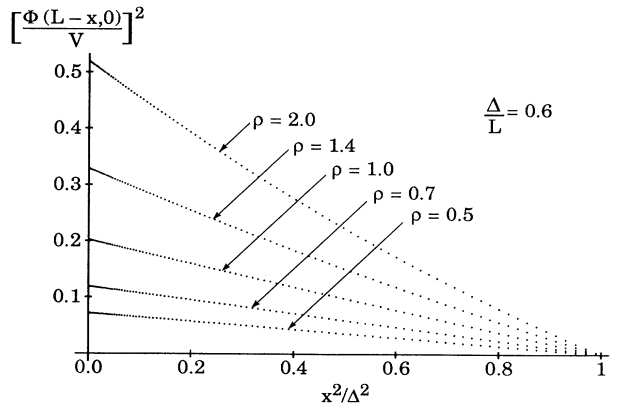

FIG. 6. $[\Phi(L-x,0)/V]^2$ vs $1-x^2/\Delta^2$ for $\rho=0.5$, 0.7, 1.0, 1.4, and 2.0.

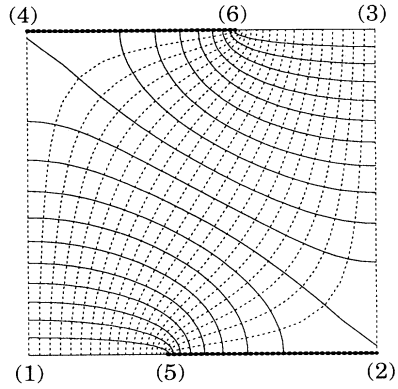

FIG. 7. Equipotential lines and current flow lines in the x,y plane for $L/H=1, \Delta/L=0.6$.

The exponential variation of $-K_1'(\rho)$ for $\rho \gtrsim 2$ suggests that ρ should be in the range from 0.5 to 2.0. Present plans are to try to use a radius as low as 1 mm, with a wall thickness of order 0.5–0.7 mm. Clearly, thermal effects will control the pulse length and duty factor of the FEL.

Finally, the slot length Δ must be chosen. Figure 6 shows a plot of $[\Phi(L-x,0)/V]^2$ versus x^2/Δ^2 for $\Delta/L=0.6$, $\rho=L/H=0.5,0.7,1.0,1.4,2.0$, suggesting strongly the proportionality

$$\Phi(L-x,0)/V \sim \sqrt{1-x^2/\Delta^2} \quad \text{for } 0 \le x \le \Delta \ . \tag{7.4}$$

Corresponding curves for other values of Δ show the same approximate linear behavior. If this is approximately correct, Q_n in Eq. (4.8) will be proportional to

$$Q_n \sim \frac{1}{L}\int_0^{\Delta} dx \sqrt{1-(x^2/\Delta^2)}\cos\left[\frac{n\pi x}{L}\right]$$

$$= \frac{1}{2n} J_1\left[\frac{n\pi\Delta}{L}\right] . \tag{7.5}$$

We now recall the need to make Q_2 vanish in order to maintain focusing in both the x and y directions. This implies

$$\frac{2\pi\Delta}{L} \cong 3.83 \ , \tag{7.6}$$

the first zero of $J_1(p)$, corresponding to $\Delta/L=0.61$. The fact that the α_0^g term in Eqs. (6.12) and (6.17) is much larger than the other terms (by a factor $A/R=\gamma/K\rho$) suggests that the tolerance on the factor Δ/L must be very tight. Specifically, since the term involving Q_2 is of order A/R times the other terms, and since K and ρ are of order 1, the accuracy required for Δ/L, on which Q_2 depends, must be a small fraction of γ^{-1}. It will probably be necessary to provide some sensitive tuning scheme to achieve the required tolerance on Q_2.

Figure 7 shows a typical plot of the equipotential and current flow lines (for $\rho=L/H=1$ and $\Delta/L=0.6$). Table I lists the values of l, h, Q_0, Q_1, Q_2, Q_3, $F_{\max}$ for $\Delta/L=0.58$, 0.60, 0.62, 0.64, 0.66 and $\rho=L/H=0.5$, 0.7, 1.0 1.4, 2.0. Table II lists the values of $K_1'(\rho)$, $\alpha^d, \alpha_0^g, \alpha^s$ for the same values of ρ. These two tables provide all the necessary information to calculate the focusing and defocusing terms in Eqs. (6.12) and (6.17) as well as $B_y^{\max}$ in Eq. (7.2). At each value of ρ it is clear that one can make $Q_2=0$ by the appropriate choice of Δ/L.

VIII. CYLINDRICAL WALL THICKNESS

Our analysis clearly assumes a wall thickness t, which is small compared to the average radius R. In the practical case, the ratio t/R may be between $\frac{1}{2}$ and 1. Moreover, we take the current distribution to be uniform in the r direction, which is only an approximation, particularly if the skin depth is comparable with t. Nevertheless, we assume that the small t/R results are a good first approximation.

In some copper tube samples which have been studied, the wall thickness turned out to be nonuniform with an approximate dependence on azimuth

$$t \cong t_0[1+\epsilon\cos(\theta-\theta_0)] \ . \tag{8.1}$$

We shall assume that ϵ is small and that the current density continues to have no r dependence. When we now determine the coefficients λ_{mn} by matching the discontinuity in H_0 to $t_0[1+\epsilon\cos(\theta-\theta_0)]J_z$, with J_z given in Eq. (5.3), it is clear that we introduce terms proportional to ϵ for $m+n$ odd. The most serious of these is the term for $m=0$, $n=1$ which we now write in the form

$$\Phi_{\text{mag}}^{01} = V\frac{\lambda_{01}\sin(\theta-\bar{\theta})}{4\rho}\begin{cases} -r/R, & r<R \\ R/r, & r>R \ . \end{cases} \tag{8.2}$$

Equating the discontinuity in $\partial\Phi_{\text{mag}}^{01}/R\,\partial\theta$ to the $m=0$, $n=1$ coefficient of $t_0[1+\epsilon\cos(\theta-\theta_0)]J_z$, we find

TABLE I. Values of $l,h,Q_n,f_{\max}$ for different $\rho,\Delta/L$.

ρ	Δ/L	l	h	Q_0	Q_1	Q_2	q_3	$f_{\max}$
0.5	0.58	0.307	0.806	0.0595	−0.0759	0.004 84	0.015 01	0.1690
0.5	0.60	0.294	0.789	0.0633	−0.0780	0.001 45	0.014 80	0.1771
0.5	0.62	0.282	0.770	0.0672	−0.0799	−0.002 05	0.014 06	0.1851
0.5	0.64	0.268	0.751	0.0712	−0.0814	−0.005 60	0.012 79	0.1929
0.5	0.66	0.255	0.730	0.0753	−0.0827	−0.009 15	0.011 04	0.2005
0.7	0.58	0.434	0.895	0.0769	−0.0982	0.006 48	0.019 28	0.1440
0.7	0.60	0.416	0.880	0.0814	−0.1003	0.002 13	0.018 91	0.1510
0.7	0.62	0.397	0.865	0.0859	−0.1021	−0.002 32	0.017 86	0.1579
0.7	0.64	0.379	0.847	0.0904	−0.1035	−0.006 77	0.016 17	0.1646
0.7	0.66	0.359	0.828	0.0950	−0.1045	−0.011 17	0.013 87	0.1711
1.0	0.58	0.640	1.067	0.1001	−0.1283	0.009 40	0.024 65	0.1094
1.0	0.60	0.613	1.057	0.1051	−0.1302	0.003 86	0.024 02	0.1149
1.0	0.62	0.585	1.045	0.1101	−0.1317	−0.001 71	0.022 54	0.1203
1.0	0.64	0.556	1.030	0.1151	−0.1326	−0.007 20	0.020 28	0.1256
1.0	0.66	0.527	1.013	0.1200	−0.1329	−0.012 54	0.017 32	0.1307
1.4	0.58	0.964	1.399	0.1270	−0.1638	0.014 00	0.030 34	0.0744
1.4	0.60	0.919	1.394	0.1323	−0.1652	0.007 31	0.029 33	0.0785
1.4	0.62	0.874	1.386	0.1374	−0.1659	0.000 70	0.027 33	0.0824
1.4	0.64	0.827	1.372	0.1424	−0.1660	−0.005 70	0.024 44	0.0862
1.4	0.66	0.780	1.355	0.1472	−0.1654	−0.011 80	0.020 79	0.0900
2.0	0.58	1.607	2.195	0.1585	−0.2060	0.020 41	0.036 75	0.0414
2.0	0.60	1.517	2.195	0.1636	−0.2064	0.012 76	0.035 14	0.0439
2.0	0.62	1.426	2.185	0.1684	−0.2060	0.005 40	0.032 43	0.0464
2.0	0.64	1.335	2.164	0.1729	−0.2048	−0.001 55	0.028 79	0.0488
2.0	0.66	1.244	2.134	0.1771	−0.2029	−0.008 03	0.024 40	0.0512

$$\lambda_{01}\cos(\theta-\bar{\theta})=\frac{2\epsilon\sigma t_0}{\pi}\rho^2[(1-4Q_0)\cos(\theta-\theta_0) -4Q_2\cos(\theta+\theta_0)] , \tag{8.3}$$

which determines both the magnitude and orientation of the new term. If we neglect the term in Q_2, which we have arranged to vanish, we find $\bar{\theta}=\theta_0$ and

$$\lambda_{01}=\frac{2\epsilon\sigma t_0}{\pi}\rho^2(1-4Q_0) . \tag{8.4}$$

Using Eq. (5.20) we find

$$\lambda_{01}=\frac{2\epsilon\sigma t_0}{\pi}\frac{\rho l}{h} . \tag{8.5}$$

The potential in Eq. (8.2) represents a constant deflecting field whose magnitude is

TABLE II. Values of $K_1'(\rho)\alpha^d,\alpha_\beta^q,\alpha^s$ for different ρ.

ρ	$K_1'(\rho)$	α^d	α_β^q	α^s
0.5	−4.237	1.116	1.180	4.674
0.7	−2.161	1.035	1.407	2.698
1.0	−1.023	1.007	1.955	1.687
1.4	−0.473	1.001	3.194	1.219
2.0	−0.184	1.000	6.800	0.961

$$B^{01}=\frac{V\lambda_{01}}{4\rho R}=\frac{\epsilon\sigma t_0 Vl}{2\pi Rh}=\frac{I\epsilon}{4\pi R} , \tag{8.6}$$

where the final form is exactly what is expected from a cylindrical shell without slots for which the centers of the inner and outer circles are a distance ϵR apart.

The order of magnitude of the deflection caused by this constant field is determined from Eq. (6.19). Specifically, we have, for the balanced focusing condition,

$$x''+\frac{1}{4A^2}x=\frac{eB^{01}}{m_0\gamma c}=\frac{e\epsilon\sigma t_0 Vl}{m_0\gamma c 2\pi Rh} , \tag{8.7}$$

so that the beam must enter the wiggler offset by

$$x_0=\frac{4A^2eB^{01}}{m_0\gamma c} . \tag{8.8}$$

Using Eqs. (8.6), (6.6), (5.10), and (7.3), we finally obtain

$$x_0=\frac{A\epsilon}{2\rho f_{\max}} . \tag{8.9}$$

Since ρ and $f_{\max}$ are of order 1, we must have $A\epsilon\ll R$ in order that the offset be small compared with the radius of the cylinder. This requires

$$\epsilon\ll\frac{R}{A}\sim\gamma^{-1} . \tag{8.10}$$

That is, the wall thickness must be uniform to an accuracy very much smaller than γ^{-1}. If such copper tubing is

not directly obtainable, some correction scheme will be necessary to compensate for a nonuniform wall thickness.

IX. SUMMARY

We have analyzed the current distribution on the surface of a thin slotted cylinder and obtained explicit expressions for the multipole expansion for the magnetic field near the axis of the cylinder. The terms in this expansion include (1) the main planar dipole wiggler field, (2) a large quadrupole term which causes focusing in one transverse direction and defocusing in the other, and (3) two somewhat smaller sextupole terms which also cause focusing in one transverse direction and defocusing in the other. The large size of the coefficient of the quadrupole term suggests that the slot length be chosen so as to make the quadrupole term vanish, or be such as to compensate for the sextupole focusing or defocusing effects.

Graphs and tables are given for the current distribution on the surface of the cylinder, and for the various multipole coefficients as a function of the two parameters:

$$\rho = (\text{circumference})/(\text{wiggler period})$$

and

$$\Delta/L = (\text{slot length})/(\text{circumference}) .$$

We show that the slot length is an extremely sensitive parameter, most likely requiring some appropriate tuning or correcting mechanism.

We have also analyzed the effect of nonuniform thickness of the cylinder wall and find that additional multipole terms are generated, including a zeroth harmonic (in the axial direction) transverse magnetic field capable of deflecting the beam transversely. Once again the effect is extremely large, suggesting the need for as uniform thickness as possible, together with some mechanism for reducing this term to an acceptably small level.

ACKNOWLEDGMENTS

The author would like to express his appreciation to Roger W. Warren for suggesting this investigation and for many illuminating conversations during the course of this work. He would also like to thank Sam Subia for preliminary numerical work and Dan Abell for the bulk of the numerical and graphical work in the paper. Finally, the author would like to thank Richard K. Cooper and AT Division at LANL, where some of the work was carried out, for its hospitality and support. This work was supported by the U.S. Department of Energy.

[1] See, for example, J. M. J. Madey, J. Appl. Phys. **42**, 1906 (1971).

[2] See, for example, K. Halbach, Nucl. Instrum. Methods **187**, 109 (1981).

[3] See, for example, J. P. Blewett and R. Chasman, J. Appl. Phys. **48**, 2692 (1977); S. Y. Park, J. M. Baird, R. A. Smith, and J. L. Hirshfield, J. Appl. Phys. **53**, 1320 (1982) for the analysis of the fields from a helical wiggler.

[4] R. W. Warren, Nucl. Instrum. Methods A **304**, 765 (1991).

[5] See, for example, J. A. Stratton, *Electromagnetic Theory* (McGraw-Hill, New York, 1941) p. 116.